# A polynomial regression approach to subpixel temperature extraction from a single-band thermal infrared image

Sarah E Paul, Carl Salvaggio
Rochester Institute of Technology, Center for Imaging Science, Digital Imaging Remote Sensing Laboratory, Rochester, NY, USA

## ABSTRACT

Target temperature estimation from thermal infrared (TIR) imagery is a complex task that becomes increasingly more difficult as the target size approaches the size of a projected pixel. At that point the assumption of pixel homogeneity is invalid as the radiance value recorded at the sensor is the result of energy contributions from the target material and any other background material that falls within a pixel boundary. More often than not, thermal infrared pixels are heterogeneous and therefore subpixel temperature extraction becomes an important capability. Typical subpixel estimation approaches make use of data from multispectral or hyperspectral sensors. These technologies are expensive and data collected by a multispectral or hyperspectral thermal imagery might not be readily available for a target of interest.

A methodology has been developed to retrieve the temperature of an object that is smaller than a projected pixel of a single-band TIR image using physics-based modeling. The process can be broken into two distinct pieces. In the first part, the Digital Imaging and Remote Sensing Image Generation (DIRSIG) tool will be used to replicate a collected TIR image based on parameter estimates from the collected image. This is done many times to build a multi-dimensional lookup table (LUT). For the second part, a regression model is built from the data in the LUT and is used to perform the temperature retrieval. The results presented are from synthetic imagery.

**Keywords:** subpixel, thermal infrared, temperature extraction, DIRSIG, lookup table, regression

## 1. INTRODUCTION AND OBJECTIVES

Previous subpixel temperature extraction methods can be divided into two categories: spectral mixture analysis and spatial disaggregation. Spectral mixture analysis starts with the equation for sensor-reaching radiance from a mixed pixel for each band of a multi-band image. Estimates of variables are obtained until the only unknowns remaining are the temperatures of the materials within the projected pixel boundary. This method requires the imagery have the at least as many bands as pixel constituents, else the system of equations is underdetermined. Dozier[1] developed a method to retrieve subpixel temperatures from a multispectral pixel containing two temperature fields as well as their areal coverage within the pixel with the requirement of knowledge of the magnitude of one of the temperature fields found within the pixel. Szymanski et al.[2] developed a method to extract the subpixel temperatures of land and water from multispectral imagery. The method requires knowledge of water and land emissivities as well as estimates of areal fractions and results were reported for synthetic data.

Spatial disaggregation leverages information from an ancillary image (e.g. a Normalized Difference Vegetation Index (NDVI) image) that is of a higher spatial resolution than the collected TIR image. The TIR image is disaggregated to the resolution of the ancillary image and the temperature is extracted from the higher resolution TIR image. Kustas et al.[3] took advantage of the relationship between radiometric surface temperatures and the NDVI to estimate subpixel vegetation temperatures. Yang et al.[4] used the genetic algorithm and self-organizing feature map (GA-SOFM) artificial neural network (ANN) to extract temperatures from a TIR image that had been disaggregated to the resolution of a VNIR image. Sentlinger et al.[5] used vectorized lake features to estimate the skin temperature for small bodies of water. The paper describes methods to gain knowledge of fractional abundances, material emissivities, and atmospheric parameters. Gustafson et al.[6] used VNIR data to sharpen TIR imagery to estimate stream temperatures. An NDVI product was derived from the VNIR image to further

Thermosense: Thermal Infrared Applications XXXIII, edited by Morteza Safai, Jeff R. Brown,
Proc. of SPIE Vol. 8013, 801302 · © 2011 SPIE · CCC code: 0277-786X/11/$18 · doi: 10.1117/12.883756

aid in the analysis.

The research mentioned above share some commonalities. One is the methods were used on naturally occurring targets with high emissivities. If the pixel material is opaque and assumed to have a high emissivity, according to Kirchhoff's Law it has a low reflectance and therefore the reflected downwelled component of sensor-reaching radiance can be considered negligible. Because of this, the downwelled term was dropped from the analysis in the works listed above save for Sentlinger et al. who came up with a rough estimate to make the method more accurate. The other similarity was that each method required multiple bands, which is also the case when performing temperature emissivity separation on multi-pixel objects.

This paper explores the possibility of retrieving subpixel temperatures for a pixel with two constituents from a single-band image using a physics-based target space approach. It is broken into two studies where the first study explores extraction results when no error is introduced into the input parameter estimates. The second study looks at the how error in one parameter estimate affects the temperature prediction. The results presented are from synthetic imagery. However, if the method was applied to a collected LWIR image it would require an independent estimate of multiple input parameters such as areal fraction, background temperature, and target and background emissivity. To get those estimates, high resolution visible imagery of the target of interest would have to be available as well. There would also have to be near perfect registration between the visible and thermal imagery. Atmospheric transmission and path radiance were not included in the synthetic imagery as it will be assumed that a collected LWIR image has been atmospherically compensated before using this method.

## 2. BACKGROUND

The physics-based portion of the physics-based target space refers to the use of a radiometrically accurate ray-tracing simulation tool to simulate a collected thermal image under a number of conditions. A target space is an N-dimensional space comprised of parameters that have a significant effect on sensor-reaching radiance as well as the sensor-reaching radiance for a pixel. In the context of this paper, the target space has two dimensions: target temperature and pixel radiance. All other parameters can be estimated from the thermal image or the high resolution visible image.

### 2.1 Thermal radiometry overview

The sensor-reaching radiance in the thermal infrared portion of the spectrum is due to multiple sources as well as the interaction between sources. Equation 1 gives the spectral sensor-reaching radiance of a homogeneous pixel for a sensor position ($\theta$, $\phi$).

$$L_{sensor}(\theta,\phi,\lambda) = \left[\varepsilon(\lambda)L_{BB}(T,\lambda) + L_r(\theta,\phi,\lambda)\right]\tau(\theta,\phi,\lambda) + L_u(\theta,\phi,\lambda) \tag{1}$$

where $\varepsilon$ is the emissivity of a material, $L_{BB}$ is the blackbody radiance for a material with temperature $T$, $L_r$ is the reflected radiance term that accounts for reflected downwelled as well as reflected background radiance from background objects, $\tau$ is the atmospheric transmission, and $L_u$ is the upwelled radiance.

The equation for sensor-reaching radiance for a mixed pixel is more complex than Equation 1 and becomes increasingly more complex with the addition of pixel constituents. The equation must now take into account not only the multiple energy sources from within the pixel but the multiple reflected components as well. This paper will only address the case of two materials (known from this point as the target and the background) within a pixel boundary. Equation 2 gives the spectral sensor-reaching radiance from a pixel with two constituents.

$$\begin{aligned} L_{sensor}(\theta,\phi,\lambda) = \left[f_t\varepsilon_t(\lambda)L_{BB}(T_t,\lambda) + f_b\varepsilon_b(\lambda)L_{BB}(T_b,\lambda) + L_{r1}(\theta,\phi,\lambda) + L_{r2}(\theta,\phi,\lambda)\right]\tau(\theta,\phi,\lambda) \\ +L_u(\theta,\phi,\lambda) \end{aligned} \tag{2}$$

where $f_t$ and $f_b$ are the areal fractions of the target and background material, respectively. The reflected radiance terms are denoted by $L_{rt}$ and $L_{rb}$ and account for the reflection of downwelled and background radiance from the target and background materials, respectively. Depending on the geometry within the pixel, the reflected term also takes into account interactions between pixel constituents. For example, a building on concrete will have reflections of the building on the concrete and vice versa. Another important parameter that is not found in Equation 2 is the position of the target within the pixel. For example, the radiance coming from a pixel with the target in the center will be different than if the target was crossing the pixel boundary. The positional information can be determined from the high-resolution visible imagery.

### 2.2 DIRSIG

The simulation tool used is the Digital Imaging and Remote Sensing Image Generation (DIRSIG) tool, which was developed by the Digital Imaging and Remote Sensing (DIRS) Laboratory at the Rochester Institute of Technology (RIT). It is a synthetic image generation application that is capable of modeling imaging systems with sensitivity in the visible through thermal infrared regions of the spectrum as well as polarimetric, RADAR, and LIDAR systems.[7] To accurately reproduce the radiometry of a scene, DIRSIG utilizes ray tracing and first principle physics, chemistry, and mathematical theories. First-principle based sub-models, including BRDF prediction, facet temperature prediction, sensor models, and atmospheric models are used to generate the synthetic imagery. All modeled components are combined using a spectral representation and integrated radiance images can be simultaneously produced for an arbitrary number of user defined bandpasses. The DIRSIG model can also incorporate multiple reflections of a photon within a simulation so that an object can interact with its surround as well as itself in the case of a complex piece of geometry. DIRSIG also handles subpixel sampling in an efficient manner via adaptive sampling.[8] This method samples based on importance, meaning it sends more samples to areas where there is more information content in the scene (e.g. edges and/or areas where the magnitude of the point spread function is large). Adaptive sampling was used to generate all of the simulations in this paper.

DIRSIG is an appropriate simulation tool to use as the physics-based modeling engine for the subpixel temperature retrieval problem for a number of reasons. One reason is its ability to handle reflected photons, which means that background reflected radiance as well as interactions within a pixel can be incorporated into a simulation. This enables complicated geometry to be modeled accurately. That capability in conjunction with the ability to interface with the atmospheric radiative transfer program, MODTRAN, to compute the downwelled radiance contribution means that the assumption of a high emissivity material does not need to be made to simplify the equation. It can also incorporate any sensor model as long as the sensor characteristics are known.

### 2.3 Linear regression analysis

Regression analysis is used to relate a dependent variable to a set of independent variables. To perform regression analysis a functional form of the relationship between the dependent and independent variables must be specified. The function might be as simple as $y = mx + b$ or as complex as a high-order polynomial with interaction terms. The specified model should always be checked for adequacy. Regardless of the choice, the model can be expressed in matrix form as

$$\mathbf{y} = \mathbf{X}\boldsymbol{\beta} + \boldsymbol{\varepsilon} \tag{3}$$

where $\mathbf{y}$ is an $n \times 1$ vector of the observations, $\mathbf{X}$ is an $n \times m$ matrix of the levels of the regressor variables and is also sometimes referred to as the design matrix, $\boldsymbol{\beta}$ is an $m \times 1$ vector of the regression coefficients, and $\boldsymbol{\varepsilon}$ is an $n \times 1$ vector of random errors.

The regression coefficients can be calculated in a number of ways but linear least squares was chosen for this effort. The least squares estimates of the regression coefficients are calculated by

$$\hat{\boldsymbol{\beta}} = \left(\mathbf{X}'\mathbf{X}\right)^{-1}\mathbf{X}'\mathbf{y} \tag{4}$$

which is the pseudoinverse of $\mathbf{X}$ multiplied by the dependent variable observations. The vector of fitted values $\hat{y}_i$ that correspond to the observed values $y_i$ is calculated by

$$\hat{\mathbf{y}} = \mathbf{X}\hat{\boldsymbol{\beta}} \tag{5}$$

The residuals are the vertical deviation of the observed dependent variables from the fitted regression line and can be expressed as

$$\mathbf{e} = \mathbf{y} - \hat{\mathbf{y}} \tag{6}$$

### 2.3.1 Model adequacy

One way of checking the adequacy of the fitted model is to look at the residuals. A plot of the residuals versus the fitted values, $\hat{y}$, can reveal common inadequacies. In the ideal case the plot would have the residuals randomly scattered in a horizontal band about zero. If, for example, a first order polynomial was being tested and the residuals revealed a polynomial shape, that would indicate that a higher-order model was required to explain all of the variation in the data set.

A second method of checking for model adequacy is to compute the number of statistically significant regression coefficients for a given model and compare that to the the next most complicated model (e.g. higher order, addition of interaction terms). If the number of significant coefficients increases, the more complex model should be used; the thought being that the a term or terms in the more complex model explain some of the variability in the data set that was not explained by the simpler model. To test for statistical significance a $t$ test is performed at a certain significance level, $\alpha$, to test the hypothesis that each coefficient is equal to zero.

## 3. METHODOLOGY

The target space described in the previous section can be thought of as infinitely continuous. In other words, the parameters can take on any value and all possible combinations of parameter values would be represented in the target space. This scenario would be optimum, but it is not physically realizable to have all possible values represented. Therefore the axes need to be bounded according to the problem at hand by making estimates of the range of likely values for the parameters using information from the scene itself. The pixel radiance is physically dependent on the target temperature and comes from the synthetic image created by DIRSIG, so the only parameter range that needs to be estimated is the target temperature. By bounding the target temperature range, the pixel radiance range will also be bounded. It is important to note that the target temperature range selected must contain the true target temperature because regression analysis does not perform well when extrapolating data.

The values of the areal fractions, material emissivities, and background temperature found in Equation 2 are known because of the use of synthetic imagery in place of a collected thermal image. In practice, the values of those parameters can be estimated from either the VIS or TIR imagery. Regardless of their source, these estimates will further bound the range of values that the pixel radiance can take on. The upwelled radiance can be neglected because of the assumption that the TIR image is atmospherically corrected. The reflected radiance terms are handled by DIRSIG.

At this point the axes in the target space have been appropriately bounded for the particular scene being interrogated. However, it is still not feasible to represent all of the possibilities so a lookup table (LUT) is generated by sampling the constrained space as illustrated in Figure 1

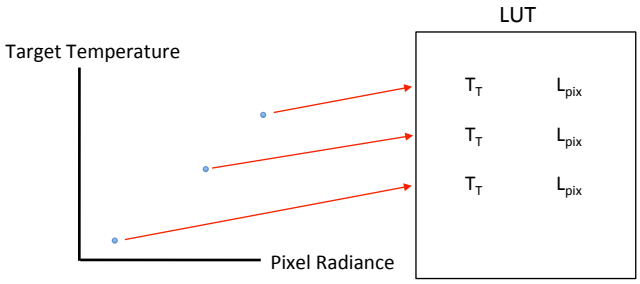


Figure 1. Example of generating the LUT by sampling the constrained target space.

It is important that the points in the LUT span the entire space uniformly so there is equal representation of the range of values.

## 3.1 Study 1: Minimum extraction error

The purpose of this study is to look at the minimum amount of temperature estimation error that can be expected from this method. This will be done by excluding error in the values of the parameters from the analysis.

### 3.1.1 Test case description

Ultimately, DIRSIG will be used to replicate a collected thermal image that contains a target of interest. The geometry of the scene will come from outside sources and will be attributed using the estimates of the areal fractions, material emissivities, background temperature, and the position of the target. For the purposes of this paper, synthetic imagery was used in place of a collected thermal image. A LWIR sensor with an integrated response function from 8 - 9.2 $\mu$m was modeled and positioned such that it was directly overhead of the target and the ground sample distance (GSD) was 1 meter. The geometry used in this study was a box on a flat surface where the box is positioned in the middle of the center pixel. A Gaussian function with a full width half max of 1 pixel was used as a point spread function. The downwelled radiance was computed by DIRSIG using radiosonde data from a sunny summer day in Buffalo, NY.

Two sets of test cases were simulated in DIRSIG with set 1 representing a manmade target ($\varepsilon_T = 0.8$) on a natural background ($\varepsilon_B = 0.98$) and set 2 representing another manmade target ($\varepsilon_T = 0.85$) on a manmade background ($\varepsilon_B = 0.9$). Five target temperatures (5°C, 35°C, 40°C, 45°C, 75°C) were used in each set as well as five target sizes (5%, 25%, 50%, 75%, and 90% of the total pixel area). The background temperature remained constant at 40 C for all test cases. This resulted in 20 test cases per set of emissivity values that spanned a wide range of physical target sizes and temperatures. Table 1 provides a summary of the values used in the simulations for the test cases.

Table 1. Summary of values used in test cases.

| **Parameter** | **Set 1 values** | **Set 2 values** |
|---|---|---|
| Target emissivity ($\varepsilon_T$) | 0.80 | 0.85 |
| Background emissivity ($\varepsilon_B$) | 0.98 | 0.90 |
| Background temperature ($T_B$) | 40°C | 40°C |
| Target temperatures ($T_T$) | 5°C, 35°C, 40°C, 45°C, 75°C | 5°C, 35°C, 40°C, 45°C, 75°C |
| Target sizes (f) | 5%, 25%, 50%, 75%, 90% | 5%, 25%, 50%, 75%, 90% |

### 3.1.2 Lookup table generation

A lookup table was generated for every target size in sets 1 and 2 making a total of 10 lookup tables. In practice, a single LUT would be generated because only one target size would come from a collected visible image of the target of interest in the LWIR image. However, one of the goals of this study was to explore the extraction error for a wide range of target sizes, thus creating the need for multiple lookup tables. The same geometry, downwelled radiance source, and point spread function were used in the construction of the LUT and the test cases. Half of the lookup tables used the emissivity values from set 1 and the other half used the emissivity values from set 2. The background temperature from Table 1 remained constant through all 10 lookup tables. The target temperatures used in each LUT ranged from 0°C to 80°C to ensure that the values in Table 1 were bracketed. Table 2 shows the parameter values used in the lookup tables.

Table 2. Values used to generate the lookup tables.

| **LUT #** | $\varepsilon_T$ | $\varepsilon_B$ | $\mathbf{T}_T$ range [°C] | $\mathbf{T}_B$ [°C] | **f** |
|---|---|---|---|---|---|
| 1 | 0.80 | 0.98 | 0 - 80 | 40 | 5% |
| 2 | 0.85 | 0.90 | 0 - 80 | 40 | 5% |
| 3 | 0.80 | 0.98 | 0 - 80 | 40 | 25% |
| 4 | 0.85 | 0.90 | 0 - 80 | 40 | 25% |
| 5 | 0.80 | 0.98 | 0 - 80 | 40 | 50% |
| 6 | 0.85 | 0.90 | 0 - 80 | 40 | 50% |
| 7 | 0.80 | 0.98 | 0 - 80 | 40 | 75% |
| 8 | 0.85 | 0.90 | 0 - 80 | 40 | 75% |
| 9 | 0.80 | 0.98 | 0 - 80 | 40 | 90% |
| 10 | 0.85 | 0.90 | 0 - 80 | 40 | 90% |

The actual values of the target temperature that were used in DIRSIG were chosen by pulling random numbers from a uniform distribution and scaling them so that they fall between the maximum and minimum temperature. We choose to use 50 values, each corresponding to a DIRSIG simulation. The same 50 temperature values were used in the generation of all 10 lookup tables, therefore 50 DIRSIG simulations were used to generate each lookup table. At the end of each simulation the target temperature along with the radiance for the pixel containing the target is recorded in the LUT.

The DIRSIG simulations can become lengthly in terms of computation time so it is advantageous to do as few runs as possible and interpolate between the values. The method chosen to interpolate the points in the LUT is linear regression.

### 3.1.3 Regression on the lookup table

Linear regression was used to interpolate between the points in the lookup table. The dependent variable was the unknown target temperature and the independent variable was the pixel radiance. A single regressor does not allow for interaction terms, so depending on the LUT used the regression model was some form of

$$T_T = \beta_0 + \beta_1 L_{pix} + \beta_2 L_{pix}^2 + \ldots + \beta_i L_{pix}^n \tag{7}$$

The regression coefficients for a first through fourth-order polynomial were computed for each data set. The fifth-order showed only a marginal decrease in extraction error ( 0.01 °C) in test cases. To decrease the likelihood of overfitting it was not used. The number of significant coefficients was computed for each model order at the $\alpha = 0.05/n$ level (where $n$ is the number of regression coefficients) and the model with the greatest number of statistically significant coefficients was selected to be the most appropriate for the data. The residuals were checked to make sure they exhibit the characteristics that indicate a satisfactory model.

Once the regression coefficients were calculated, the radiance from the pixel containing the target in each test case was used as an input to the regression equation from the lookup table that was constructed using the same emissivity set and target size. To calculate the extraction error, the extracted target temperature was subtracted from the truth target temperature.

## 3.2 Study 2: Adding parameter error

The purpose of this study was to analyze how error in a single parameter estimate affects the temperature extraction error.

### 3.2.1 Test case description

Eight sets of parameters were use to generate synthetic imagery test cases for the error study. The test cases represent eight collected LWIR images. Table 3 show the values for each parameter.

Table 3. Parameter values for the eight test cases used in the error analysis study.

| **Test case #** | $\varepsilon_T$ | $\varepsilon_B$ | $\mathbf{T}_T$ [°C] | $\mathbf{T}_B$ [°C] | **f** |
|---|---|---|---|---|---|
| 1 | 0.85 | 0.95 | 55 | 40 | 50% |
| 2 | 0.85 | 0.85 | 55 | 40 | 50% |
| 3 | 0.90 | 0.90 | 55 | 40 | 50% |
| 4 | 0.80 | 0.90 | 55 | 40 | 50% |
| 5 | 0.85 | 0.90 | 55 | 44 | 50% |
| 6 | 0.85 | 0.90 | 55 | 36 | 50% |
| 7 | 0.85 | 0.90 | 55 | 40 | 64% |
| 8 | 0.85 | 0.90 | 55 | 40 | 36% |

The same geometry and sensor that were used in the first study were used to generate the synthetic DIRSIG images. The same point spread function and downwelled radiance data were used as well.

### 3.2.2 Lookup table generation

A single LUT was constructed with the parameters found in Table 4 using the same geometry and sensor set up that has been used all along in conjunction with the application of the same point spread function and downwelled radiance contribution from the test cases.

Table 4. Parameter values used to construct the LUT for the error study.

| **Parameter** | **Value** |
|---|---|
| $\varepsilon_T$ | 0.85 |
| $\varepsilon_B$ | 0.90 |
| $\mathrm{T}_T$ range [°C] | 0 - 80 |
| $\mathrm{T}_B$ [°C] | 40 |
| f | 50% |

This LUT represents the values of the best estimates of the parameters used in the eight test cases. So, for example, the background emissivity from case 1 would effectively be underestimated in the LUT by 0.05 units whereas the background emissivity value from case 2 would effectively be overestimated by 0.05 units. All other parameters contain no error in their estimate in the LUT. Table 5 provides a summary of the error introduced by the lookup table.

Table 5. A summary of the amount of error introduced into the process by the values in the lookup table either overestimating or underestimating a single parameter from each test case. It should be noted that the ±14% error introduced into the target size assumes a 5:1 resolution ratio between a visible image and an LWIR image set.

| Case # | Error introduced by LUT |
|---|---|
| 1 | $\varepsilon_B$ - 0.05 |
| 2 | $\varepsilon_B$ + 0.05 |
| 3 | $\varepsilon_T$ - 0.05 |
| 4 | $\varepsilon_T$ + 0.05 |
| 5 | $T_B$ - 4°C |
| 6 | $T_B$ + 4°C |
| 7 | f - 14% |
| 8 | f +14% |

The amount that the LUT overestimates and underestimates each test case was chosen to so that the amount of error in the parameter estimates would represent typical errors expected when exploiting collected imagery.

### 3.2.3 Regression on the lookup table

Regression coefficients were computed for the lookup table. The radiance of the pixel containing the target was recorded from each test case image and the regression coefficients were applied to calculate an extracted target temperature value. To calculate the extraction error, the extracted target temperature was subtracted from the truth target temperature.

## 4. RESULTS

### 4.1 Study 1 results

The first study looked at the minimum amount of temperature extraction error for targets spanning a wide range of physical sizes as well as temperatures. Figure 2 contains plots of the extraction error versus the target size. Each marker symbol represents a different target temperature that corresponds to those found in Table 1. Figure 2(a) is a plot of the extraction error for the values in set 1 from Table 1 and Figure 2(b) is the extraction error for the values in set 2.

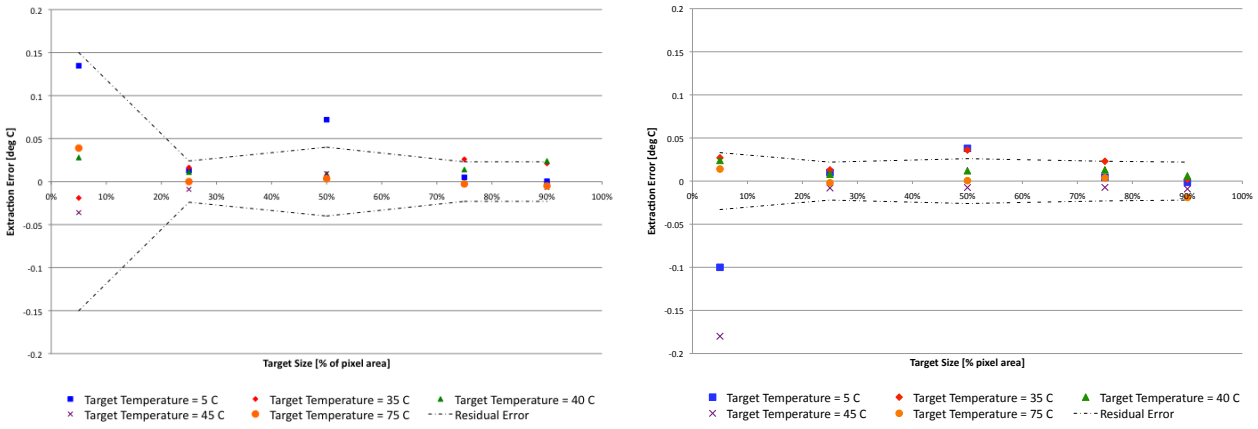


(a) $T_B = 40°C$, $\varepsilon_T = 0.8$, $\varepsilon_B = 0.98$ (b) $T_B = 40°C$, $\varepsilon_T = 0.85$, $\varepsilon_B = 0.9$

Figure 2. Plot of temperature extraction error [°C] vs target size for a nominal manmade material on a natural surface 2(a) as well as for a nominal manmade material on a manmade surface 2(b). Each marker shape represents the extraction error for a different target temperature.

The dotted black line on each plot represents one positive and negative standard deviation of the residuals for each lookup table. The standard deviation of the residuals was plotted as a line instead of discrete points for the sake of visibility. With a few exceptions, the extraction error in Figures 2(a) and 2(b) is contained within the bounds of the standard deviation of the residuals. This makes sense, since for this study, the only error in the process comes from the regression model itself. In short, the extraction error in the plots depicted in Figure 2 represent the error in the regression model. Therefore it is not possible to compare extraction error between target sizes within one plot, as well as between the plots, or to glean any other information in terms of trends in the data.

### 4.2 Study 2 results

The extraction errors for each test case are found in Table 6.

Table 6. Summary of temperature extraction errors for each test case.

| **Test case #** | **Extraction error [°C]** |
|---|---|
| 1 | -2.90 |
| 2 | 2.77 |
| 3 | -3.11 |
| 4 | 2.98 |
| 5 | -6.43 |
| 6 | 6.30 |
| 7 | -3.19 |
| 8 | 2.85 |

The extraction errors were around ± 3 °C with the exception of cases 6 and 7 where the background estimates were the source of error. The importance of the background temperature as an error source should decrease as the target size increases. Conversely, it should increase as the target size decreases. The temperature extraction error for the case when a parameter was overestimated was similar to the extraction error when the parameter was underestimated. This indicates that this method will behave in the same manner regardless of which direction (increasing or decreasing) the estimation error goes.

We believe the amount of error that was introduced to be a reasonable estimate of what one would see while exploiting collected imagery. However, this error analysis was by no means comprehensive as only one source of error was introduced per test case. The exploitation of collected imagery would have multiple parameter estimates that containing error silumtaneously. This study served to start to identify how the error on a single parameter affected the overall temperature extraction error as well as to determine if one or more parameters stood out as large contributors to the overall error.

## 5. SUMMARY

This paper explored the possibility of extracting the temperature of a target that is smaller than a pixel using a physics-based target space approach. The method assumes that there are only two constituents within a pixel and all results were from synthetic imagery that was generated by the DIRSIG modeling application. The first study presented looked at the minimum error that could be expected when this method is implemented for a wide range of target sizes and target temperatures. It was determined that when no error is present in the estimations of the parameters, the temperature extraction error was solely do to the error in the regression model. The second study saw the introduction of error to the estimate of one parameter per test case. The amount of error introduced into each parameter is what was believed to be reasonable for exploitation of real imagery. The extraction errors were around ±3 °C with the exception of the cases where the background temperature estimate was the source of error.

## 6. ACKNOWLEDGEMENTS

This work was carried out using funding received from the United States Department of Energy under BAA PDP08 Grant Number DE-AR52-07NA28115. Thanks also goes to the Research Computing group at RIT for maintaining the computer cluster used to run the simulations.

## REFERENCES

1. J. Dozier, "A method for satellite identification of surface temperature fields of subpixel resolution," *Remote Sensing of Environment* , pp. 221 – 229, 1981.
2. J. J. Szymanski, C. C. Borel, Q. O. Harberger, P. Smolarkiewicz, and J. P. Theiler, "Subpixel temperature retrieval with multispectral sensors," in *Algorithms for Multispectral and Hyperspectral Imagery V*, **3868**, pp. 478–486, 1999.
3. W. P. Kustas, J. M. Norman, M. C. Anderson, and A. N. French, "Estimating subpixel surface temperatures and energy fluxes from the vegetation index-radiometric temperature relationship," *Remote Sensing of Environment* , 2003.
4. G. Yang, R. Pu, W. Huang, J. Wang, and C. Zhao, "A novel method to estimate subpixel temperature by fusing solar-reflective and thermal-infrared remote-sensing data with an artificial neural network," *Geoscience and Remote Sensing, IEEE Transactions on* **48**(4), pp. 2170 – 2178, 2010.
5. G. I. Sentlinger, S. J. Hook, and B. Laval, "Sub-pixel water temperature estimation from thermal-infrared imagery using vectorized lake features," *Remote Sensing of Environment* **112**, pp. 1678 – 1688, 2008.
6. W. T. Gustafson, R. N. Handcock, and A. R. Gillespie, "An image-sharpening method to recover stream temperatures from aster images," in *Remote Sensing for Environmental Monitoring, GIS Applications, and Geology II*, M. Ehlers, ed., **4886**, pp. 72–83, SPIE, 2003.
7. Digital Imaging and Remote Sensing Laboratory, Rochester, NY, *The DIRSIG User's Manual*, 2008.
8. S. E. Paul, A. A. Goodenough, S. D. Brown, and C. Salvaggio, "Sub-pixel radiometry: A three-party study in generating synthetic imagery that incorporates sub-pixel variation," in *Algorithms and Technologies for Multispectral, Hyperspectral, and Ultraspectral Imagery XVI*, **7695**, SPIE, 2010.